

# On the discrete nature of the Red Giant Branch of $\omega$ Centauri <sup>\*</sup>

A. Sollima<sup>1,2</sup> †, F. R. Ferraro<sup>1</sup>, E. Pancino<sup>2</sup>, M. Bellazzini<sup>2</sup>

<sup>1</sup> *Dipartimento di Astronomia, Università di Bologna, via Ranzani 1, Bologna, Italy*

<sup>2</sup> *Osservatorio Astronomico di Bologna, via Ranzani 1, I-40127 Bologna, Italy*

Accepted 2004 January 00. Received 2004 January 00; in original form 2004 January 00

## ABSTRACT

We report the results of an extensive VLT high-resolution imaging campaign of the central region of the giant globular cluster  $\omega$  Centauri. More than 100,000 stars have been measured in the inner  $9' \times 9'$  region of the cluster. On the basis of multiband Colour Magnitude Diagrams (CMD), we confirm the existence of multiple stellar populations along the Red Giant Branch (RGB). Moreover, thanks to the high-precision of this dataset, we conclude that the RGB does not present a smooth and continuous distribution, but shows a discrete structure: besides the metal-poor and the extreme metal-rich population (RGB-a), the existence of three metal intermediate populations is shown.

**Key words:** techniques: photometric – stars: evolution – stars: Population II – globular cluster:  $\omega$  Cen.

## 1 INTRODUCTION

The understanding of the star formation history of the globular cluster  $\omega$  Centauri (NGC 5139) represents one of the most interesting challenges of stellar astrophysics.  $\omega$  Cen is the most massive and luminous GC of the Milky Way ( $M \sim 2.9 \cdot 10^6 M_{\odot}$ , Merrit et al. 1997) and it is surely the most peculiar in terms of structure, kinematics and stellar content. One of the most interesting peculiarities of  $\omega$  Cen is its metallicity spread. The first sign of chemical inhomogeneity was found by Dickens & Woolley (1967) from the large colour width of the Red Giant Branch (RGB) in the colour-magnitude diagram (CMD). This result was later confirmed by a large number of spectroscopic works (Freeman & Rodgers 1975, Butler, Dickens & Epps 1978).

In the last ten years, extensive spectroscopic surveys have been performed on large samples of giant stars (Norris, Freeman & Mighell 1996, hereafter NFM96; Suntzeff & Kraft 1996, hereafter SK96), showing a multimodal heavy-element distribution. Recent wide-field photometric studies (Lee et al. 1999, Pancino et al. 2000 - hereafter P00, Hilker & Richtler 2000, Hughes & Wallerstein 2000, Rey et al. 2004) have revealed the presence of an additional, well defined anomalous RGB (hereafter RGB-a). According to P00, this population contains approximately 5% of the cluster's

stellar content and represents the extreme metal-rich end of the observed metallicity distribution. Moreover, the metal-rich giants appear to have different spatial distribution and dynamical behaviour with respect to the metal poor ones (Pancino et al. 2000, 2003, Jurcsik 1998, Norris et al. 1997).

In this framework, we have started a long-term project devoted to the detailed study of the properties of the different stellar populations in this cluster (see Ferraro, Pancino & Bellazzini 2002), based on a complete multi-wavelength photometric survey and an extensive spectroscopic campaign for giant and subgiant stars, both in the optical and in the infrared bands. Within this project, a number of results have been published on the photometric, chemical and kinematic properties of the RGB-a stars (see Pancino et al. 2000, 2002, 2003; Ferraro et al. 2002; Sollima et al. 2004; Origlia et al. 2002, 2003) and the possible detection of its Sub Giant Branch (SGB, Ferraro et al. 2004).

In this paper we present BVI photometry of more than 100,000 stars in the central region of the cluster <sup>1</sup>. In §2 we describe the observations, the data reduction techniques and the photometric calibration. In §3 we present the CMD, describing the main characteristics of the different cluster populations. In §4 the photometric metallicity distribution for a large sample of red giants is presented and discussed. In §5 we show the detection of the RGB bumps of the different

<sup>\*</sup> Based on FORS observations collected with the Very Large Telescope at the European Southern Observatory, Cerro Paranal, Chile, within the observing program 68.D-0332.

† E-mail: antonio.sollima@bo.astro.it

<sup>1</sup> The entire catalog is only available in electronic form at the CDS via anonymous ftp to cdsarc.u-strasbg.fr (130.79.128.5) or via <http://cdsweb.u-strasbg.fr/>

populations of  $\omega$  Cen. Finally, we summarize and discuss our results in §6.

## 2 OBSERVATIONS AND DATA REDUCTION

The photometric data were obtained with the FORS1 camera, mounted at the Unit1 (UT1) of the Very Large Telescope (VLT) of the ESO (Cerro Paranal, Chile). All observations were performed in Service Mode in 5 different nights on March, April and June 2002 (see Table 1), using the high resolution mode of FORS1. In this configuration the image scale is  $0.1'' \text{ pixel}^{-1}$  and the camera has a global field of view of  $3.4' \times 3.4'$ . A mosaic of 9 ( $3 \times 3$ ) partially overlapping fields has been observed around the cluster center, covering a total area of  $\sim 9' \times 9'$ , (see Figure 1).

After applying the standard bias and flat-field correction, we used DAOPHOT II and the point-spread-function (PSF) fitting algorithm ALLSTAR (Stetson, 1987) to obtain instrumental magnitudes for all the stars detected in each frame. For each field, six different frames have been observed (4 long and 2 short-exposure) through the B, V and I filters. Repeated exposures have been combined in order to obtain a high signal-to-noise median image. The automatic detection of sources was performed on the median frame adopting a  $3\sigma$  threshold. The mask with the object positions was then used as input for the PSF-fitting procedure, that was performed independently on each image. As usual, the most isolated and bright stars in each field have been employed to build the PSF model (here a Moffat function of exponent 2.5). For each passband, the magnitudes obtained from the long exposures were transformed to the same instrumental scale and averaged. The same procedure was followed for the short exposures, that were however used only to measure bright stars, which are saturated in the long exposures. The calibrating equations linking the instrumental magnitudes to the standard system were obtained from the comparison with the photometric catalog by Pancino et al. (2000, 2003). Finally, a catalog with more than 100,000 calibrated stars in the cluster has been produced. Our calibration has been compared with the photometric catalog by Rey et al. (2004) in the B and V passbands. The mean magnitude differences found are  $\Delta B = 0.069 \pm 0.066$  and  $\Delta V = 0.060 \pm 0.054$ , which are consistent with a small systematic offset in both passbands.

### 2.1 Photometric errors

The root mean square (rms) frame-to-frame scatter of instrumental magnitudes computed for each star from repeated exposures is a good indicator of the internal photometric accuracy. Figure 2 reports the distribution of photometric errors in different passbands as a function of magnitude. As expected, the errors significantly increase towards faint magnitudes, due to photon noise.

We used this diagram in order to define a high-accuracy sample (hereafter HA sample) that contains only stars with the lowest rms. The behaviour of photometric errors has been modelled, as a function of magnitude, with analytical functions, adopting the curves that provide  $\sigma_{r.m.s} = 0.01$  at

**Table 1.** Observing logs

| Field | Date           | Filter | Exp time<br>(sec) | Seeing (FWHM)<br>(") |
|-------|----------------|--------|-------------------|----------------------|
| 1     | 14-15 Jun 2002 | B      | 299               | 0.6                  |
| 1     | 14-15 Jun 2002 | B      | 10                | 0.6                  |
| 1     | 14-15 Jun 2002 | V      | 45                | 0.6                  |
| 1     | 14-15 Jun 2002 | V      | 2                 | 0.6                  |
| 1     | 14-15 Jun 2002 | I      | 25                | 0.6                  |
| 1     | 14-15 Jun 2002 | I      | 1                 | 0.6                  |
| 2     | 13-14 Jun 2002 | B      | 299               | 0.6                  |
| 2     | 13-14 Jun 2002 | B      | 10                | 0.6                  |
| 2     | 13-14 Jun 2002 | V      | 45                | 0.6                  |
| 2     | 13-14 Jun 2002 | V      | 2                 | 0.6                  |
| 2     | 21 Apr 2002    | I      | 25                | 0.8                  |
| 2     | 21 Apr 2002    | I      | 1                 | 0.8                  |
| 3     | 14-15 Jun 2002 | B      | 299               | 0.6                  |
| 3     | 14-15 Jun 2002 | B      | 10                | 0.6                  |
| 3     | 14-15 Jun 2002 | V      | 45                | 0.6                  |
| 3     | 14-15 Jun 2002 | V      | 2                 | 0.6                  |
| 3     | 14-15 Jun 2002 | I      | 25                | 0.6                  |
| 3     | 14-15 Jun 2002 | I      | 1                 | 0.6                  |
| 4     | 13-14 Jun 2002 | B      | 299               | 0.6                  |
| 4     | 13-14 Jun 2002 | B      | 10                | 0.6                  |
| 4     | 13 Jun 2002    | V      | 45                | 0.6                  |
| 4     | 13 Jun 2002    | V      | 2                 | 0.6                  |
| 4     | 20 Apr 2002    | I      | 25                | 0.6                  |
| 4     | 20 Apr 2002    | I      | 1                 | 0.6                  |
| 5     | 11 Mar 2002    | B      | 299               | 0.6                  |
| 5     | 11 Mar 2002    | B      | 10                | 0.6                  |
| 5     | 11 Mar 2002    | V      | 45                | 0.6                  |
| 5     | 11 Mar 2002    | V      | 2                 | 0.6                  |
| 6     | 11 Mar 2002    | B      | 299               | 0.6                  |
| 6     | 11 Mar 2002    | B      | 10                | 0.6                  |
| 6     | 11 Mar 2002    | V      | 45                | 0.6                  |
| 6     | 11 Mar 2002    | V      | 2                 | 0.6                  |
| 6     | 11 Mar 2002    | I      | 25                | 0.6                  |
| 6     | 11 Mar 2002    | I      | 1                 | 0.6                  |
| 7     | 14-15 Jun 2002 | B      | 299               | 0.6                  |
| 7     | 14-15 Jun 2002 | B      | 10                | 0.6                  |
| 7     | 14-15 Jun 2002 | V      | 45                | 0.6                  |
| 7     | 14-15 Jun 2002 | V      | 2                 | 0.6                  |
| 7     | 14-15 Jun 2002 | I      | 25                | 0.6                  |
| 7     | 14-15 Jun 2002 | I      | 1                 | 0.6                  |
| 8     | 11 Mar 2002    | B      | 299               | 0.6                  |
| 8     | 11 Mar 2002    | B      | 10                | 0.6                  |
| 8     | 11 Mar 2002    | V      | 45                | 0.6                  |
| 8     | 11 Mar 2002    | V      | 2                 | 0.6                  |
| 8     | 11 Mar 2002    | I      | 25                | 0.6                  |
| 8     | 11 Mar 2002    | I      | 1                 | 0.6                  |
| 9     | 13-14 Jun 2002 | B      | 299               | 0.6                  |
| 9     | 13-14 Jun 2002 | B      | 10                | 0.6                  |
| 9     | 13-14 Jun 2002 | V      | 45                | 0.6                  |
| 9     | 13-14 Jun 2002 | V      | 2                 | 0.6                  |
| 9     | 13-14 Jun 2002 | I      | 25                | 0.6                  |
| 9     | 13-14 Jun 2002 | I      | 1                 | 0.6                  |

B=18, V=18 and I=17. To construct the HA sample, only stars with errors below these curves have been considered. Figure 2 shows the selection performed on the global catalog: stars included in the HA sample are marked with heavy black dots.

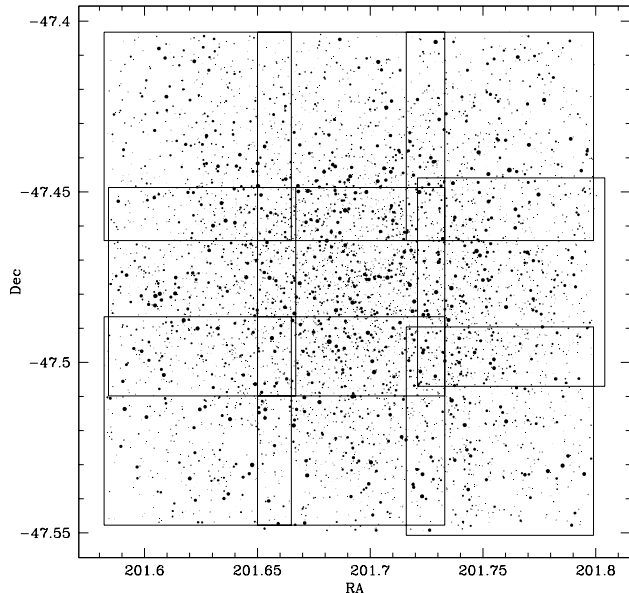


**Figure 1.** Map of the region sampled by the observations. North is up, east on the right. Only stars with  $V < 16$  have been plotted.

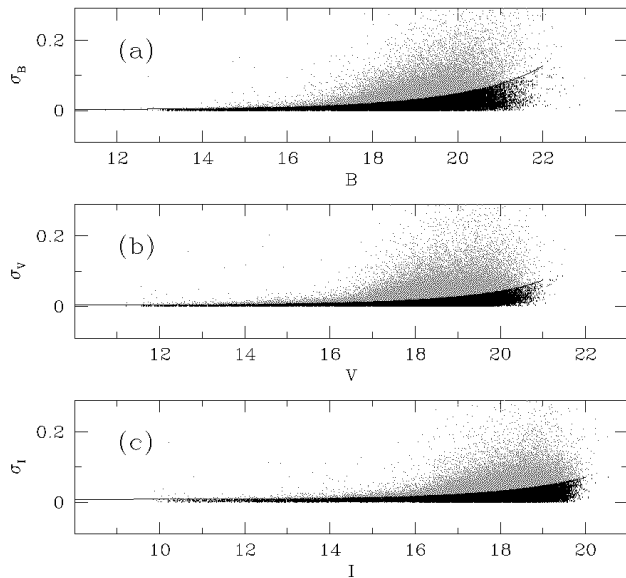


**Figure 2.** B (panel a), V (panel b) and I (panel c) photometric errors as a function of magnitude. Grey points represent measurements excluded from the high-accuracy sample.

### 3 COLOR - MAGNITUDE DIAGRAMS

Figures 3 and 4 show the  $(V, B - V)$  and  $(I, B - I)$  CMDs for the global sample of stars measured in  $\omega$  Cen. Figure 5 shows the  $(V, B - V)$  CMD for the high-accuracy sample, where a more precise analysis of the sequences is possible. The main features of the presented CMDs are schematically listed below:

- (i) The CMDs sample the entire evolved population in the cluster, reaching the upper Main Sequence (MS) at  $V \sim 20$ ;
- (ii) The anomalous RGB (RGB-a, as defined by P00), is also visible as a well separated population at the extreme red side of the main RGB structure;
- (iii) A complex structure of the intermediate RGB components (RGB-MInt(s)), which populate the CMD region between the RGB-MP and the RGB-a, can also be noticed;
- (iv) A narrow, well-defined Sub Giant Branch which merges into the MS of the dominant cluster population is visible in Figure 5, at a magnitude level significantly fainter than the MS Turn-Off (this feature is described and discussed in Ferraro et al. 2004).

Apart from the anomalous SGB, the most surprising feature of the CMDs shown in Figures 3, 4 and 5 is the *discrete structure* of the intermediate RGBs. The complex morphology of the RGB has been already noted in several recent publications (e.g. Lee et al. 1999, P00 and Rey et al. 2004). However, in all the above studies, the RGB-MInt population appears to uniformly populate the CMD region delineated by the dominant RGB-MP population and the recently discovered RGB-a.

In the CMDs presented here instead a discrete, comb-like structure becomes evident, with a set of different intermediate RGB-MInt(s) populating the region between the RGB-MP and the RGB-a. Figure 6 shows a selection of RGB stars, done on the high-accuracy sample, at three different magnitude levels ( $V = 13, 13.5$  and  $14$  respectively). The corresponding colour distributions are shown in three adjacent panels. As can be seen, five peaks can be identified: the two extreme peaks being the RGB-MP and the RGB-a, while three additional peaks can be distinguished between them (RGB-MInt(s)).

This discrete structure of the RGB has strong implications for the chemical evolution of  $\omega$  Cen, and suggests a star formation history characterized by bursts, as will be discussed in §7.

### 4 METALLICITY DISTRIBUTION FUNCTION

It is well known that the RGB colour of an old Simple Stellar Population (SSP) is mainly affected by the abundance of heavy elements and only to a lesser extent by the age of the population. The effect of age differences becomes smaller and smaller with increasing age, and for population II stars it can be neglected. Therefore, we used the RGB colour distribution to derive a metallicity distribution function (MDF – see also Bellazzini et al, 2003). For this purpose, we selected a sub-sample of stars from the HA sample in the  $(V, B - V)$  plane, having  $V < 14.6$ ,  $B - V > 0.75$  (see Figure 7), in order to limit the analysis to the region in which colour is most sensitive to metallicity. We took special care in excluding HB and AGB stars, which are easily identified from the high quality CMDs shown in Figures 3, 4 and 5.

We then compared the selected RGB stars with a grid of ridge lines of galactic globular cluster (GGC), having different metallicities, taken from the sample of Ferraro et al. (1999 – hereafter F99). A metallicity estimate was derived for each star by interpolating the grid of templates in the  $(V, B - V)$  plane. A similar approach was adopted by Frinchaboy et al. (2002, hereafter Fr02) who compared the

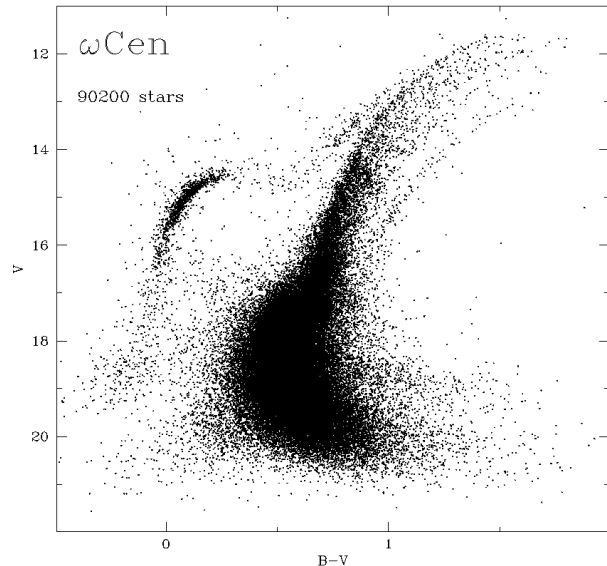


**Figure 3.**  $(V, B - V)$  color-magnitude diagram for the global sample of  $\sim 90,000$  stars measured in  $\omega$  Cen.

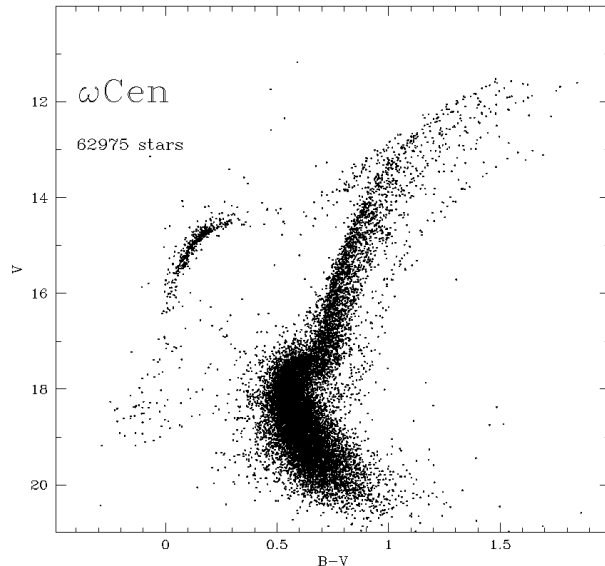


**Figure 5.**  $(V, B - V)$  color-magnitude diagram for selected stars in the high-accuracy sample (the HA sample).

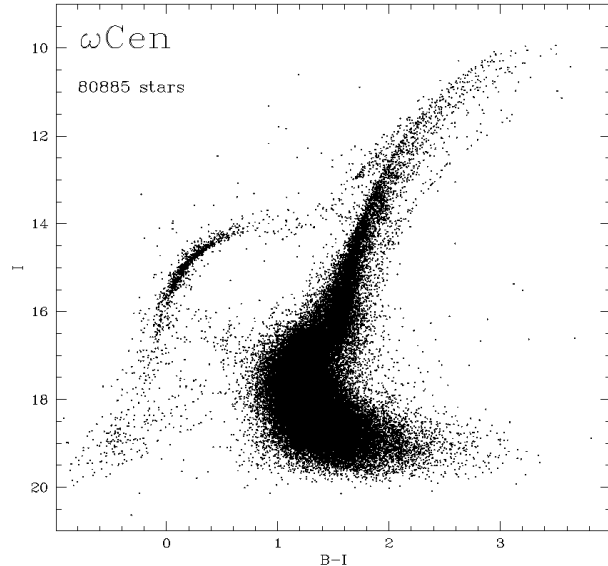


**Figure 4.**  $(I, B - I)$  color-magnitude diagram for the global sample of  $\sim 80,000$  stars measured in  $\omega$  Cen.

RGB star distribution from the Washington  $M, T_2$  photometry with theoretical isometallicity curves. Also Lee et al. (1999) and P00 obtained empirical MDFs in  $\omega$  Cen by calibrating, in terms of metallicity, the distance of each giant from the mean ridge line of the main metal-poor component (RGB-MP). Finally, Hilker & Richtler (2000) derived the photometric metallicity for a large sample of stars using  $vby$  Strömgren photometry and the related metallicity indices. In the following we analyze in detail the obtained MDF and compare our results with those of the authors quoted above

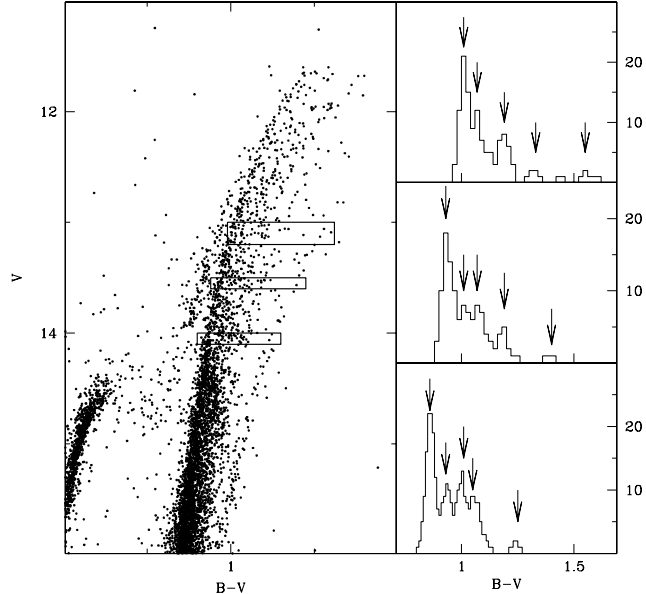


**Figure 6.** RGB colour distribution at different magnitude levels ( $V = 13, 13.5$  and  $14$  respectively), as marked on the left panel. 5 different peaks are evident in the right panels, marked by arrows.

and with the existing spectroscopic works of NFM96 and SK96.

#### 4.1 Basic assumptions

In order to compare the RGB stars distribution with the mean ridge lines from F99, we need to assume a distance modulus and a reddening correction. In the following we

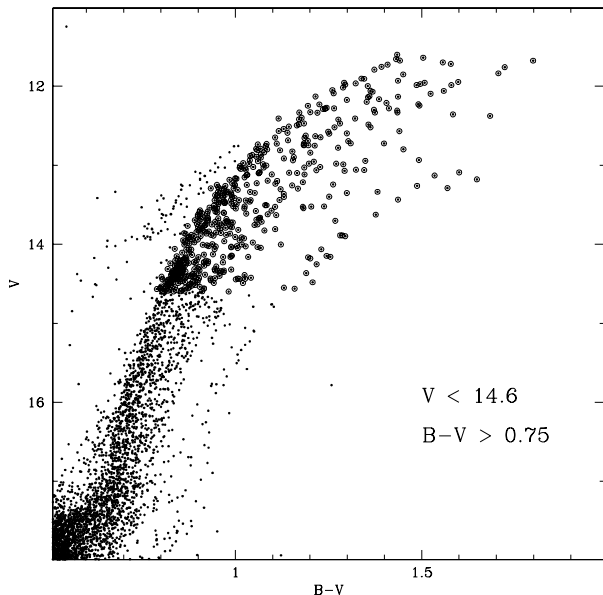


**Figure 7.** The zoomed part of the high-accuracy ( $V, B-V$ ) CMD in the RGB region. Stars selected to derive the MDF are marked with open circles.

adopt the distance modulus by Thompson et al. (2001)  $(m - M)_0 = 13.65 \pm 0.11$  based on the observations of the detached eclipsing binary system OGLE GC17. Concerning the reddening and extinction coefficients, we assumed  $E(B - V) = 0.11 \pm 0.01$  (Lub, 2002),  $A_B = 4.1E(B - V)$  and  $A_V = 3.1E(B - V)$  (Savage & Mathis, 1979).

In our analysis, we considered the global metallicity scale adopted by F99. Straniero & Chieffi (1991) and Salaris, Chieffi & Straniero (1993) showed that, when computing the isochrones of Population II stars, the contribution of the  $\alpha$ -element enhancement can be taken into account by simply rescaling standard models to the global metallicity  $[M/H]$ , according to the following relation

$$[M/H] = [Fe/H] + \log_{10}(0.638 10^{[\alpha/Fe]} + 0.362) \quad (1)$$

Direct measurements of the  $\alpha$ -elements abundance in halo and disk field stars have shown a very well defined behavior as a function of  $[Fe/H]$ , with a nearly constant overabundance ( $[\alpha/Fe] \sim 0.3$ ) for  $[Fe/H] < -1$ , and an evident trend with metallicity, which linearly decreases to  $[\alpha/Fe] \sim 0.0$  as metallicity increases (see Edvardsson et al. 1993, Nissen et al. 1994, Magain 1989, Zhao & Magain 1990, Gratton et al. 1996). Since there is evidence (Pancino et al. 2002, Origlia et al. 2003) that the stellar populations in  $\omega$  Cen have different  $\alpha$ -element enhancement levels, the global metallicity  $[M/H]$  is the most appropriate quantity to consider in the present case.

## 4.2 Results

Figure 8 shows the obtained MDF for 540 stars in the HA sample (*panel a*) and for 1,364 stars in the global sample (*panel b*), with  $V < 14.6$ ,  $B-V > 0.75$ . The distributions are clearly asymmetric: beside the main peak, in both cases

other four peaks are well visible. They can be associated with the following components:

- (i) The dominant metal poor population RGB-MP with  $[M/H] \simeq -1.4$ ;
- (ii) Three different metal intermediate components at  $[M/H] \simeq -1.2$  (RGB-Mint1),  $[M/H] \simeq -0.9$  (RGB-Mint2) and  $[M/H] \simeq -0.7$  (RGB-Mint3), respectively;
- (iii) The anomalous population RGB-a is clearly visible as a sharp peak at the extreme of the distribution (at  $[M/H] \simeq -0.5$ ).

In order to check the validity of this approach, we compared our metallicity estimates with those obtained with the Ca Triplet survey by NFM96 (with the 41 stars in common). To convert the metallicities presented by NFM96 into the global scale, we first converted the equivalent widths of NFM96 into the Rutledge et al. (1997) system, and derived the iron abundance in the Carretta & Gratton (1997) scale (see Section 5 in Rutledge et al. 1997).

Then the derived metallicities have been converted into the global metallicity scale  $[M/H]$  using the eq. (1). According to Ferraro et al. (1999), we assumed  $[\alpha/Fe] = +0.28$  for stars with  $[Fe/H]_{CG} < -0.8$  and  $[\alpha/Fe] = -0.35[Fe/H]_{CG}$  for stars with  $[Fe/H]_{CG} > -0.8$  (see F99). The comparison of NFM96 metallicities transformed adopting this procedure with our photometric metallicities is shown in Figure 9. As can be seen, the agreement is quite good. The solid line shown in Figure 9 represents the iso-metallicity relation. The bottom panel shows the residuals of the comparison. The nice agreement between the two metallicity determinations is confirmed within the errors, with a mean dispersion of  $\sigma_{[M/H]} \simeq 0.2$  dex.

The MDF shown in Figure 8 (a) is in good agreement with those presented by the other photometric surveys (Lee et al. 1999, P00 and Fr02). The peak detected at  $[M/H] \simeq -0.5$  was not found by Fr02, probably because, as pointed out by the author, their catalog is severely incomplete in the inner 6 arcmin, a region where the anomalous metal rich RGB-a seems to be concentrated (see P00 and Pancino et al. 2003, hereafter P03). With respect to the spectroscopic works (NFM96 and SK96) and the photometric estimates by Hilker & Richtler (2000) we note that, while the global shape of the MDFs are similar, the metal rich components of the distribution presented in this paper are not reproduced. The lack of metal rich stars in the distributions of NFM96 and SK96 is probably due to two different effects: (i) the different mean radial distances of the samples: NFM96 and SK96 limit their analysis to outer regions of the cluster where the presence of RGB-a stars is less evident. (ii) the magnitude selection adopted by NFM96 ( $V < 13$ ), which tends to exclude RGB-a stars. Note that a few RGB-a stars are visible in the extreme red portion of the CMD selection boxes of SK96. Hilker & Richtler (2000) found a distribution similar to that of NFM96, with a continuous high-metallicity tail at  $[Fe/H] > -0.8$ . The different structure found at high-metallicities is probably due to the dependence of the Strömgren photometric metallicity index on CN abundance, which is not linearly dependent on metallicity.

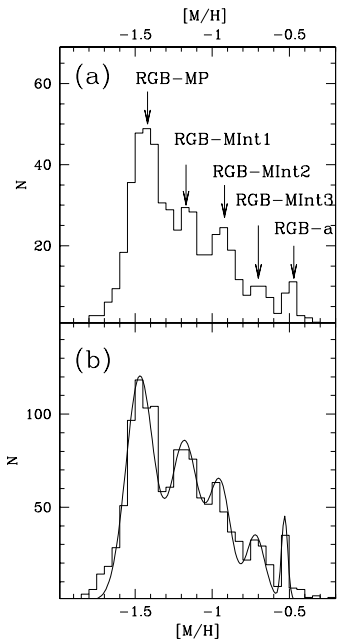


**Figure 8.** The derived MDF for the high-accuracy (a) and for the global sample (b). The significant peaks of the distribution are indicated in *panel a* and interpolated with a multi-burst enrichment model (*panel b*).

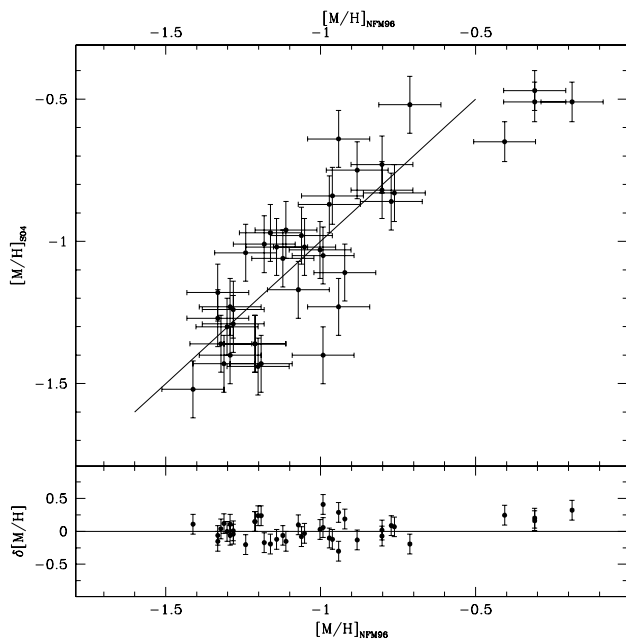


**Figure 9.** Comparison between the metallicities derived in this paper with those obtained by NFM96 for the 41 common stars (top panel). The residuals of the comparison are also shown (bottom panel). A solid line in both panels shows the iso-metallicity locus as a reference.

### 4.3 Statistical significance of the peaks

As quoted above, the MDF shown in Figure 8 suggests the existence of 5 peaks. Following the procedure described by NFM96, we assumed that the chemical evolution of a stellar system can be well represented by a simple model of chemical enrichment (Searle & Sargent 1972, Hartwick 1976, Zinn 1978, NFM96). This model considers the evolution of a cloud of gas having initial abundance  $Z_0$ , which experiences instantaneous recycling of the ejecta from massive supernovae, and from which gas is expelled at a rate proportional to the star formation rate. Under these assumption the form of the abundance distribution is

$$f(Z) = \sum_{i=1}^N f_i(Z)$$

where

$$f_i(Z) = \frac{I_i e^{-(Z-Z_{0i})/(\langle Z_i \rangle - Z_{0i})}}{\langle Z_i \rangle - Z_{0i}} \quad \text{for } Z > Z_{0i}$$

$$f_i(Z) = 0 \quad \text{elsewhere}$$

Where  $I_i$  represents the intensity of the  $i$ -th star formation burst.

In order to estimate the significance of the revealed peaks, we fit the derived MDF with this model, following the prescription of NFM96. Assuming  $[M/H] = \log(Z/Z_{\odot})$ , we converted  $f(Z)$  into a function of the global metallicity  $f([M/H])$  and smoothed it with a gaussian kernel of  $\sigma=0.05$  (equal to the width of the MDF bin, Zinn 1978). We therefore performed a maximum likelihood analysis of the data (see appendix B(c) of Morrison, Flynn & Freeman 1991). We treated the fit in terms of three free parameters for each burst: initial metallicity  $Z_{0i}$ , average metallicity  $\langle Z_i \rangle$  and burst intensity  $I_i$ .

The choice of the number  $N$  of bursts in the model must be done by balancing *bias* and *variance* of the fit: a small number of components leads to an uncertain fit, while large values of  $N$  lead to a more stable fit, that however might contain unnecessary components. For this purpose, we used the *Bayesian Information Criterion* (BIC – Schwarz, 1978). Let  $n$  ( $=32$ ) be the bins of the MDF shown in Fig. 8 (a),  $p$  ( $=3N$ ) the free parameters of the fit and  $\ell_N$  the log-likelihood function at the maximized parameters values

$$\ell_N = \log L_N = \sum_{j=1}^n \log Pr_{j,N}$$

Where  $Pr_{j,N}$  represents the probability that the number of stars whose metallicity lies in the  $j$ -th bin of the MDF be drawn from a  $N$ -bursts distribution. Then we choose  $N$  to maximize the quantity

$$BIC(N) = \ell_N - \frac{p}{2} \log n$$

We observe that  $BIC(N)$  reaches its maximum value when  $N=4$ . This implies that the observed peaks in the MDF shown in Fig. 8 (a) are most probably reproduced by a four component model.

The above analysis of the peak's significance is entirely based on a simple model of self enrichment. However, there is observational evidence suggesting that the case of  $\omega$  Cen can be much more complex than this (Norris et al. 1997). In particular, recent results cast some doubts on the hypothesis

**Table 2.** Relative frequency of the main populations of  $\omega$  Cen

|           | [M/H] | %      |
|-----------|-------|--------|
| RGB-MP    | -1.4  | 42 ± 8 |
| RGB-MInt1 | -1.2  | 28 ± 6 |
| RGB-MInt2 | -0.9  | 17 ± 5 |
| RGB-MInt3 | -0.7  | 8 ± 3  |
| RGB-a     | -0.5  | 5 ± 1  |

that the RGB-a was the direct result of a self-enrichment process within  $\omega$  Cen (Pancino et al. 2002, Ferraro et al. 2002, 2004). In the following discussion, we will extend our analysis to all of the five components as they appear from the histograms in Figures 6 and 8, and we reserve to further address the statistical significance of each of them in the future. We will also treat and discuss the RGB-a separately, whenever needed.

In order to estimate the relative frequency of each population, we computed the area covered by each single burst distribution  $f(Z_i)$ . Since the selection performed on the HA sample could have corrupted the relative population ratios, we use the global sample. The results of the fit are plotted over the histograms in Figure 8 (b) and summarized in Table 2, where the peak metallicity and the relative frequency are listed for each considered population. We note that the extreme metal-rich population (RGB-a) represents  $\sim 5\%$  of the stars of the whole system, fully in agreement with P00 and P03. Regarding the metal poor population, its relative frequency is significantly smaller than the estimate of P03 ( $\sim 70\%$ ), while the Mint(s) populations represent a consistent fraction of the whole system with respect to what established by P03 ( $\sim 25\%$ ). This effect is most probably due to the contamination of the RGB-MInt1 on the RGB-MP sample of P03, whose photometry did not allow a clear separation between the two.

#### 4.4 Spatial distribution

Using the RGB samples defined in the previous section, we investigated the spatial distributions of the sub-populations. In order to minimize the contamination between the metal-poor and MInts populations we limited our analysis to the brightest portion of the RGBs ( $V < 16$ , see Fig. 10). We computed the surface density distributions of each sample using an adaptive kernel estimator algorithm (Fukunaga 1972, Silvermann 1986, Beers 1991, Merrit & Tremblay 1994). However, the smaller area covered by the photometry presented here, and the subdivision in five components, drastically reduce the number size of each sample so that only a qualitative discussion can be done on the resulting spatial distributions. The comparison of the observed distributions reveals that both the MInts and RGB-a stars present a distribution that significantly differs from the RGB-MP sample's one. A two-dimensional generalization of the Kolmogorov-Smirnov test (Peacock 1983, Fasano & Franceschini 1987) gives a probability that the spatial distribution of the co-added (RGB-MInts + RGB-a) sample and the RGB-MP one are drawn from the same parent distribution of less than 0.2 %. These results confirm those of P00, P03 and NFM96. Table 3 reports the location of

**Table 3.** RGB centroids

|       | RA<br>(deg) | Dec<br>(deg) | $\delta$ RA<br>(deg) | $\delta$ Dec<br>(deg) | d<br>(") | N    |
|-------|-------------|--------------|----------------------|-----------------------|----------|------|
| MP    | 201.703     | -47.4711     | –                    | –                     | –        | 1132 |
| MInt1 | 201.694     | -47.4865     | -0.009               | -0.0154               | 60       | 637  |
| MInt2 | 201.686     | -47.4850     | -0.017               | -0.0139               | 64       | 411  |
| MInt3 | 201.744     | -47.4669     | 0.041                | 0.0042                | 101      | 244  |
| RGB-a | 201.691     | -47.4551     | 0.012                | 0.0160                | 65       | 133  |

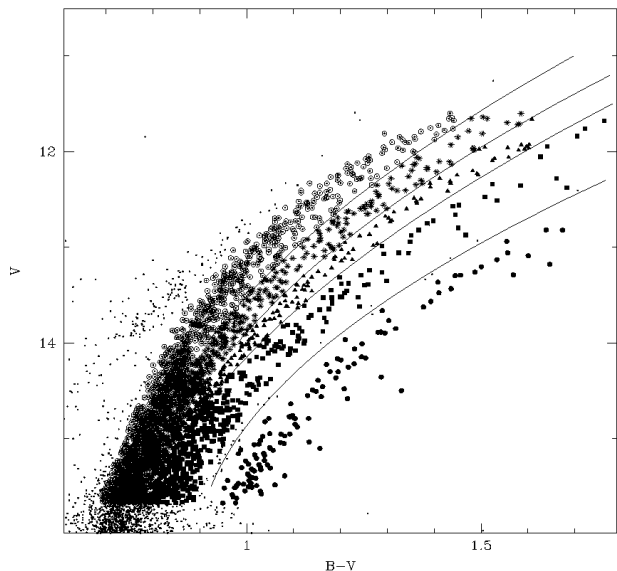


**Figure 10.** Groups selection in the global  $(V, B - V)$  CMD. The different population samples are marked with different symbols. The continuous lines follow the distribution minima and are used to separate the groups.

the centroids, the distance from the dominant population (RGB-MP) center and the number size of the sample for the different population of  $\omega$  Cen. We observe that, while the centroid of the MInt1 sample is located close to the dominant MP component center, the three most metal rich populations (RGB-MInt2, RGB-MInt3 and RGB-a) seem to have different centroids. In particular, the RGB-a centroid appears displaced  $\sim 61''$  to the north of the dominant population, in full agreement with P03.

## 5 THE RED GIANT BRANCH BUMPS

One of the most interesting features of the RGB is the so-called RGB bump (Iben, 1968). The location of the RGB bump in the CMD is mainly a function of age and metal content of a given stellar population. Because of the age-metallicity differences between the populations of  $\omega$  Cen, one expects that this feature will appear in each RGB at a fainter magnitude as metallicity increases. The identification of the RGB bump is not an easy task because of the need of large observational samples (Crocker & Rood 1984, Fusi Pecci et al. 1990).

To identify the RGB bump in our CMD we performed

the procedure described in the following. By computing the colour distribution of stars at different magnitude levels along the RGB in the global  $(V, B - V)$  CMD, we separated the five populations of  $\omega$  Cen by following the position of the distribution minima (see Fig. 10). Then we located the RGB bumps by identifying the corresponding peaks in the differential RGB luminosity functions (LF). Figures 10 and 11 shows the five RGB groups and their corresponding LFs, respectively. The bumps for the RGB-MP and RGB-Mint populations are clearly defined and marked with arrows, while the RGB bump of the extreme metal rich population (RGB-a) is much less evident and will be not considered in the following discussion. In Table 4 the observed  $V_{Bump}$  magnitudes for the four considered populations of  $\omega$  Cen are listed.

It is interesting to note that the location of the RGB bumps on our CMD does not appear as a "continuous and slanting feature", as it was described by Rey et al., (2004) but as a succession of distinct peaks. This is best put into evidence in Figure 12, where the Hess diagram constructed on a zoomed area of the  $(V, B - V)$  CMD is presented. As can be seen, the bumps are clearly separated from each other, again pointing towards a set of well separated components in the RGB of  $\omega$  Cen.

The absolute magnitudes of the RGB-bumps are plotted as a function of the photometric metallicities, obtained in Sect. 4, in panel a of Figure 13. The result is compared to the empirical relation of F99 (obtained from the detection of the RGB-bump in 54 GGC) and to the theoretical expectation by Straniero, Chieffi & Limongi (1997, hereafter SCL97), computed for  $Y = 0.23$  and age= 16 Gyr. As can be seen (Figure 13), the location of the RGB bump for the four considered populations of  $\omega$  Cen is in agreement, within the uncertainties, with the predictions of both relations. This further supports the calibration of the derived MDF discussed in Sect. 4 and the discrete nature of the RGB components in  $\omega$  Cen.

In panel (b) of Fig. 13 the positions of the bumps are compared with isochrones in the plane  $M_V^{bump}$  vs.  $[M/H]$  derived from the SCL97 models (Eq. 3 of F99). Neglecting the actual zero point of the resulting age-scale, that may strongly depend on the details of the theoretical models (see also Riello et al. 2003), the distribution of the observed points over the isochrones grid suggests an age range of several Gyr between the MP and the most metal-rich MInt populations. While still within the observational uncertainties, the observed trend deserves some discussion, since it provides independent support to the results obtained from the analysis of Turn-Off stars with Strömgren photometry by Hughes et al. (2004), and with medium resolution spectroscopy by Hilker et al. (2004).

The derived age range ( $\sim 6$  Gyr) has to be considered as a strong upper limit because of (a) the unrealistically old zero-point of the age scale (18 Gyr) and (b) the neglect of the Helium enrichment which should be associated with the process that altered the mean metallicity from  $[M/H] \simeq -1.4$  to  $[M/H] \simeq -0.7$ . The more metal rich bumps plotted in Fig. 13 appear brighter than that expected if they were associated with population having the same age and He content of the MP population. Since both a younger age and an increase in He abundance (Y) should enhance the luminosity of the bumps, the observed trend may be in-

**Table 4.** RGB bump parameters of  $\omega$  Cen

| RGB bump | $V_{bump}$       | $[M/H]$        |
|----------|------------------|----------------|
| MP       | $14.31 \pm 0.03$ | $-1.4 \pm 0.2$ |
| MInt1    | $14.42 \pm 0.03$ | $-1.2 \pm 0.2$ |
| MInt2    | $14.57 \pm 0.03$ | $-0.9 \pm 0.2$ |
| MInt3    | $14.84 \pm 0.04$ | $-0.7 \pm 0.2$ |

terpreted either in terms of age and/or Y variations. In this context, several authors considered the effects of differences in helium abundance between the different populations of  $\omega$  Cen (Ferraro et al. 2004, Bedin et al. 2004, D’Antona & Caloi 2004, Norris 2004). In particular, Norris (2004) suggested a helium enhancement of  $\delta Y \sim 0.10 - 0.15$  in order to reproduce the complex MS-TO morphology of  $\omega$  Cen. SCL97 models predict

$$\frac{\delta M_V^{Bump}}{\delta Y} \sim -2.45$$

Assuming that the MInt2 population corresponds to the "second population" of Norris (2004) (having  $\Delta[M/H]=0.5$  with respect to the dominant MP population), the observed difference in the RGB bump level between these populations can be induced by an helium enhancement of  $\Delta Y \sim 0.09$ , once the effect due to the metallicity has been taken into account and assuming no age difference between these populations. This finding is not too far from what proposed by Norris (2004), but should be considered as an upper limit if we accept that MInt2 population is younger than MP one, as suggested by elementary concepts of chemical evolution. The most reasonable hypothesis is that both factors are contributing, according to the natural trend of chemical evolution, e.g. successive generations of stars are younger than the MP population and more enriched in metals and He.

In panel (c) of Fig. 13 the differential Age-Metallicity Relation (AMR) obtained from panel (b) is displayed ( $\Delta$  age = 0.0 is placed at age= 18 Gyr). This plot shows that the AMR derived from the RGB bumps is very similar to that obtained by Hughes et al. (2004) and it is fully compatible with the same "closed box" model adopted by these authors (see their Fig. 7). The above comparisons strongly indicate that there is full compatibility between the constraints obtained from the TO region of the CMD by Hughes et al. (2004) and Hilker et al. (2004). and the observed trend in the  $M_V^{bump}$  vs.  $[M/H]$  described in the present paper. Both results suggest that the chemical enrichment of the  $\omega$  Centauri system in the range  $-1.4 \leq [M/H] \leq -0.7$  occurred on a timescale of a few Gyr ( $< 6$  Gyr), the actual value depending on the unknown amount of Helium enrichment.

## 6 DISCUSSION AND CONCLUSIONS

We presented high precision BVI photometry for  $\omega$  Cen, resulting from an accurate survey of the cluster’s core. More than 100,000 stars have been measured, allowing a complete characterization of the RGB. In particular, the most robust conclusion of our work is that *the complex structure of  $\omega$  Cen RGB does not show a smooth and continuous distribution of populations, but it has a clearly discrete structure.* At least four, most probably five, separate components

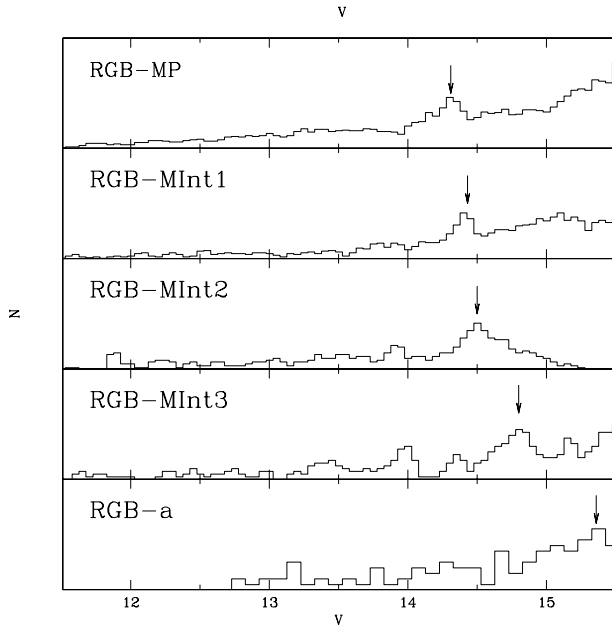


**Figure 11.** Differential LFs for five RGB groups. The peaks corresponding to the RGB bumps are marked with arrows. In the upper panel the groups selection in the  $(V, B-V)$  CMD is shown.

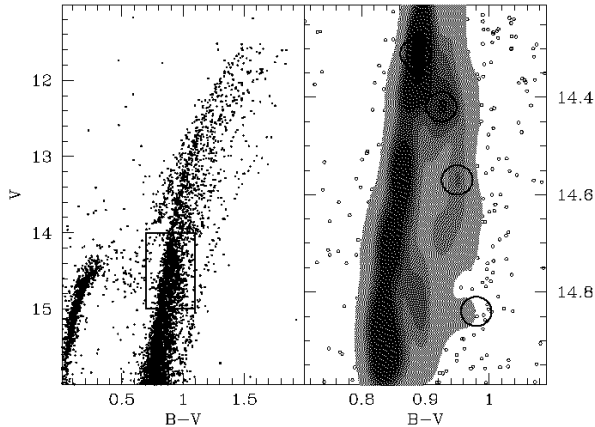


**Figure 12.** Hess diagram for the RGB bump region marked in the left panel. In the right panel, the location of the RGB bump for the MP and the three MInts populations is marked with open circles.

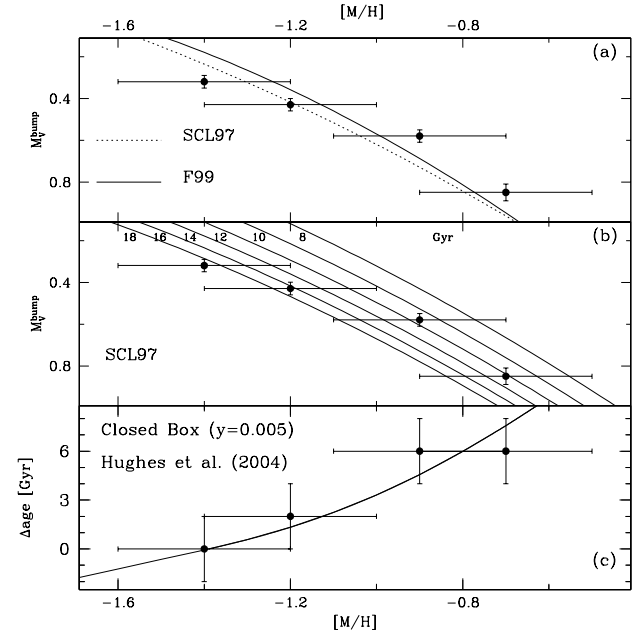


**Figure 13.** Panel (a):  $M_V$  of the RGB bumps as a function of global metallicity  $[M/H]$ . The solid line is the empirical relation by F99, the dashed line is the theoretical prediction by the Straniero, Chieffi & Limongi (1997) models at  $t=16$  Gyr. Panel (b): Comparison with the isochrones in the  $M_V$  vs  $[M/H]$  plane. The isochrones are derived from the same models that adopt a fixed He abundance of  $Y = 0.23$  (see F99). Panel (c): Age-Metallicity Relation obtained from the bumps. The thick continuous line is the AMR predicted by the same “closed box” model adopted by Hughes et al. (2004), assuming constant star formation and yield  $y = 0.005$ .

have been identified. The discreteness and different nature of the components, clearly visible from the new CMD presented (Fig. 7), has been further demonstrated by studying in detail: (i) the photometric metallicity distribution function, which shows five separate peaks (see Fig. 8) and (ii) the identification of the RGB bump for each population (although some uncertainty remains on the RGB-a bump), which appear as distinct peaks if studied through a Hess diagram (Fig. 12), and indicate an age difference of  $\sim 6$  Gyr between the MP and the most metal-rich MInt population.

Such a characteristic has one simple implication on the star formation history of  $\omega$  Cen, if interpreted from the point of view of a simple self-enrichment scenario. It implies in fact that each population of  $\omega$  Cen (except maybe the RGB-a, see below) can be associated with a different episode of star formation. Therefore, the chemical evolution of  $\omega$  Cen should be viewed as a series of bursts, separated in time. However, a *simple* self-enrichment scenario may not be the best description of the evolution of  $\omega$  Cen. We recall at this point the puzzling correlations between chemical and kinematical properties found by Freeman (1985) and Norris et al. (1997). Also from the chemical point of view  $\omega$  Cen shows some peculiarities which are not observed in normally self-enriching systems, i.e. dwarf galaxies and the field of the Milky Way. One such characteristic is the presence of CH-CN, Na-O, Mg-Al anomalies (Norris & Da Costa 1995a), which up to now has only been observed in galactic glob-

ular clusters,  $\omega$  Centauri and nowhere else. The second is the strong enhancement of s-process elements seen in both the metal-poor and intermediate components (Evans 1983, Norris & Da Costa 1995b, Smith et al. 2000, Vanture et al. 2002) and the RGB-a (Pancino 2003) of  $\omega$  Centauri. This last peculiarity has only been observed in another stellar system, the Sagittarius dwarf galaxy, which is presently merging with the Milky Way. Therefore, a simple self-enrichment cannot explain all the observational evidences gathered in the past, in particular when the RGB-a population is considered. In fact it appears to stand out from the other populations in terms of morphology, structure, chemical composition and kinematics. The RGB-a main peak appears significantly dislocated from the main population's one. Moreover, the RGB-a chemical abundance, besides the higher iron content, presents a smaller  $\alpha$ -enhancement with respect to the other populations (Pancino et al. 2002, P03, Origlia et al. 2003) while a large overabundance of heavy neutron capture elements remains high as for the other populations (Pancino 2003). Finally, the mean proper motion of the RGB-a stars appears significantly different from that of the main cluster population (Ferraro et al. 2002). This last result have been questioned by Platais et al. (2003) who claimed that the different proper motion observed for the RGB-a is due to a spurious instrumental effect in the original proper motion catalog by van Leeuwen et al. (2000). However, while the arguments claimed by Platais et al. (2003) were already considered and dismissed in the original publication by van Leeuwen et al. (2000), they also have been strongly criticized by Hughes et al. (2004) who emphasised that no evidence of systematic trend has been detected in the proper motion residuals. Further support to the correctness of the proper motion measurements has been brought by Pancino (2003), who again did not found any significative residual trend as a function of either magnitude or color.

Summarizing, the whole body of evidence points towards a complex scenario, where the different populations could have not only had a different chemical enrichment history, but also a *different dynamical evolution*. It is clear that if one desires to accommodate all the observational facts in one self-consistent scenario, it is necessary to include not only a complex chemical evolution, but also a complex dynamical history, possibly including minor mergers within a framework such as the "merger within a fragment" (Searle 1977, Norris et al. 1997), or capture of smaller components.

## ACKNOWLEDGMENTS

This research was supported by the Agenzia Spaziale Italiana and the Ministero dell'Istruzione, dell'Università e della Ricerca. We warmly thank Paolo Montegriffo for assistance during the catalogs cross-correlation and astrometric calibration procedure and Santino Cassisi and Oscar Straniero for the helpful scientific discussion. We also thank John E. Norris, the Referee of our paper, for his precious comments and suggestions.

## REFERENCES

- Bedin, L. R., Piotto, G., Anderson, J., Cassisi, S., King, I. R., Momany, Y. & Carraro, G., 2004, ApJ, 605, L125
- Beers, T.C., Forman, W., Huchra, J.P., Jones, C., Gebhardt, K., 1991, AJ, 102, 1581
- Bellazzini, M., Cacciari, C., Federici, L., Fusi Pecci, F., Rich, M., 2003, A&A, 405, 867
- Butler, D., Dickens, R. J. & Epps, E. A., 1978, ApJ, 225, 148
- Carretta, E. & Gratton, R., 1997, A&AS, 121, 95
- Crocker, D.A., Rood R.T., 1984, in "The Observational Tests of the Stellar Evolution Theory", ed. A. Maeder & Renzini (Dordrecht:Reidel),159
- D'Antona, F., Caloi, V., 2004, ApJ, 611, 871
- Dickens, R. J. & Woolley, R., 1967, R. Obs. Bull., 128, 255
- Edvardsson, B., Andersen, J., Gustafsson, B., Lambert, D. L., Nissen, P. E. & Tomkin, J. 1993, A&A, 275, 101
- Evans, T. L., 1983, MNRAS, 204, 975
- Fasano, G. & Franceschini, A., 1987, MNRAS, 225, 155
- Ferraro, F.R., Messineo, M., Fusi Pecci, F., De Palo, M.A., Straniero, O., Chieffi, A. & Limongi, M., 1999, AJ, 118, 1738
- Ferraro, F. R., Pancino, E., Bellazzini, M., in "A Unique Window into Astrophysics", 2002, ed. F. van Leeuwen, J.D.Huges & G.Piotto, ASP Conf.Series, 407
- Ferraro, F. R., Bellazzini, M., Pancino, E., 2002, ApJ, 573, 95
- Ferraro, F. R., Sollima, A., Pancino, E., Bellazzini, M., Origlia, L., Straniero, O., Cool, A., 2004, ApJ, 603, L81
- Freeman, K. C. & Rodgers, A. W., 1975, ApJ, 201, L71
- Freeman, K. C. , 1975, IAU Symp. "Dynamics of Star Clusters" , 113, 33
- Frinchaboy, P. M., Rhee, J., Ostheimer, J. C., Majewski, S. R., Patterson, R. J., Johnson, W. Y., Dinescu, D. I., Palma, C., Westfall, K. B., in "A Unique Window into Astrophysics", 2002, ed. F. van Leeuwen, J.D.Huges & G.Piotto, ASP Conf.Series, 143
- Fusi Pecci, F., Ferraro, F.R., Crocker, D., Rood, R.T. & Buonanno, R., 1990, A&A 238, 95
- Fukunaga, K., 1972, Introduction to Statistical Pattern Recognition, Academic Press, New York
- Gratton, R., Carretta, E., Matteucci, F. & Sneden, C. 1996, in "The Formation of the Galactic Halo . . . Inside and Out", ed. H. L. Morrison & A. Sarajedini (San Francisco: ASP), 307, ASP Conf.Ser. 92
- Hartwick, F. D. A., 1976, ApJ, 209, 418
- Hilker, M., Richtler, T., 2000, A&A, 362, 895
- Hilker M., Kaiser A., Richtler T. & Willemsen, P., 2004, A&A, 422, 9
- Hughes, D. W., Wallerstein, D. P., 2000, AJ, 119, 1225
- Hughes J., Wallerstein G., van Leeuwen F., Hilker M., 2004, AJ, 127, 980
- Iben, I.Jr., 1968, Nature, 220, 143
- Jurcsik, J., 1998, ApJ, 506, 113
- Lee, Y. W., Joo, J. M., Sohn, Y. J., Rey, S. C., Lee, H. C. & Walker, A. R., 1999, Nature, 402, 55
- Lub J. in "A Unique Window into Astrophysics", 2002, ed. F. van Leeuwen, J.D.Huges & G.Piotto, ASP Conf.Series, 95
- Magain, P. 1989, A&A, 209, 211
- Merritt, D., Meylan, G. & Mayor, M., 1997, AJ, 114, 1074

- Merritt, D., Tremblay, B., 1994, AJ, 108, 514
- Morrison, H. L., Flynn, C., Freeman, K. C., 1991, AJ, 110, 1191
- Nissen, P. E., Gustafsson, B., Edvardsson, B. & Gilmore, G. 1994, A&A, 285, 440
- Norris, J. E., Da Costa, G. S., 1995a, ApJ, 441, 81
- Norris, J. E., Da Costa, G. S., 1995b, ApJ, 447, 680
- Norris, J. E., Freeman, K. C. & Mighell, K. J., 1996, ApJ, 462, 241
- Norris, J. E., Freeman, K. C., Mayor, M. & Seitzer, P., 1997, ApJ, 487, L187
- Norris, J. E., 2004, ApJ, 612, L25
- Origlia, L., Ferraro, F. R., Rood, R., Fusi Pecci, F., 2002, ApJ, 571, 458
- Origlia, L., Ferraro, F.R., Bellazzini, M., Pancino, E., 2003, ApJ, 591, 916
- Pancino, E., Ferraro, F. R., Bellazzini, M., Piotto, G. & Zoccali, M., 2000, ApJ, 534, L83
- Pancino, E., Pasquini, L., Hill, V., Ferraro, F. R. & Bellazzini, M., 2002, ApJ, 568, L101
- Pancino, E., Seleznev, A., Ferraro, F. R., Bellazzini, M. & Piotto, G., 2003, MNRAS, 345, 683
- Pancino, E., 2003, PhD Thesis, Bologna University
- Peacock, J. A., 1983, MNRAS, 202, 615
- Platais, I., Wyse, R. F. G., Hebb, L., Lee, Y. W. & Rey, S. C., 2003, ApJ, 591, L127
- Rey, S. C., Lee, Y. W., Ree, C. H., Joo, J. M., Sohn, Y. J. & Walker, A. R., 2004, AJ, 127, 958
- Riello M., Cassisi S., Piotto G., Recio-Blanco A., De Angeli F., Salaris M., Pietrinferni A., Bono G., Zoccali M., 2003, A&A, 410, 553
- Rutledge, G. A., Hesser, J. E., Stetson, P. B., Mateo, M., Simard, L., Bolte, M., Friel, E. D., Copin, Y., 1997, PASP, 109, 883
- Rutledge, G. A., Hesser, J. E., Stetson, P. B., 1997, PASP, 109, 907
- Salaris, M., Chieffi, A., Straniero, O., 1993, Mem. Soc. Astron. Italiana, 63, 315
- Savage, B.D., Mathis, J.S., 1979, ARA&A, 17, 73
- Schwarz, G., 1978, Annals of Statistics, 6,461
- Searle, L., Sargent, W. L. W., 1972, ApJ, 173, 25
- Searle, L., 1977, in *The Evolution of Galaxies and Stellar Populations*, ed. B. M. Tinsley & R. B. Larson (New Haven: Yale Univ. Obs.), 219
- Silvermann, B. V., in "Density Estimator for Statistics and Data Analysis", 1986, ed. Chapman & Hall, New York
- Smith, V. V., Suntzeff, N. B., Cunha, K., Gallino R., Busso, M., Lambert, D. L. & Straniero, O., 2000, AJ, 119, 1239
- Sollima, A., Ferraro, F. R., Origlia, L., Pancino E. & Bellazzini, M., 2004, A&A, 420, 173
- Stetson, P. B., 1987, PASP, 99, 191
- Straniero, O., Chieffi, A., 1991, ApJS, 76, 911
- Straniero, O., Chieffi, A. & Limongi, M., 1997, ApJ, 490, 425
- Suntzeff, N. B. & Kraft, R. P., 1996, AJ, 111, 1913
- Thompson, I.B., Kaluzny, J., Pynch, W., Burley, G., Krzeminski, W., Paczynski, B., Persson, S.E. & Preston, G.W., 2001, AJ, 121, 3089
- van Leeuwen, F., Le Poole, R. S., Reijns, R. A., Freeman, K. C., & de Zeeuw, P. T., 2000, A&A, 360, 472
- Vanture, A. D., Wallerstein, G. & Suntzeff, N. B., 2002, ApJ, 569, 984
- Zhao, G. & Magain, P. 1990, A&A, 238, 242
- Zinn, R., 1978, ApJ, 225, 790